Chemosphere 307 (2022) 135922

Contents lists available at ScienceDirect

Chemosphere

journal homepage: www.elsevier.com/locate/chemosphere

Reusable composite membranes for highly efficient chromium removal from real water matrixes

J.M. Queirós [a,b,c,1], H. Salazar [a,b,d,1], A. Valverde [f], G. Botelho [d], R. Fernández de Luis [d,*], J. Teixeira [a,b,d], P.M. Martins [c,e,**], S. Lanceros-Mendez [f,g]

[a] Physics Centre of Minho and Porto Universities (CF-UM-UP), University of Minho, 4710-057, Braga, Portugal
[b] LaPMET - Laboratory of Physics for Materials and Emergent Technologies, University of Minho, 4710-057, Braga, Portugal
[c] Centre of Molecular and Environmental Biology, University of Minho, 4710-057, Braga, Portugal
[d] Centre/Department of Chemistry, University of Minho, 4710-057, Braga, Portugal
[e] IB-S – Institute for Research and Innovation on Bio-Sustainability, University of Minho, 4710-057, Braga, Portugal
[f] BCMaterials, Basque Center for Materials, Applications and Nanostructures, UPV/EHU Science Park, 48940, Leioa, Spain
[g] IKERBASQUE, Basque Foundation for Science, 48009, Bilbao, Spain

HIGHLIGHTS

- The removal of Cr^{VI} through adsorption requires time and cost intensive sorbent's recovery and reactivation.
- Sorbent nanoparticles immobilization into polymeric membranes offers a solution to overcome these drawbacks.
- Inactivation of the sorbent when immobilized into the polymeric matrix is a key parameter to assess their performance.
- If the encapsulation of the sorbents is minimized, hybrid membranes are easy recovered, reactivated and functional.

GRAPHICAL ABSTRACT

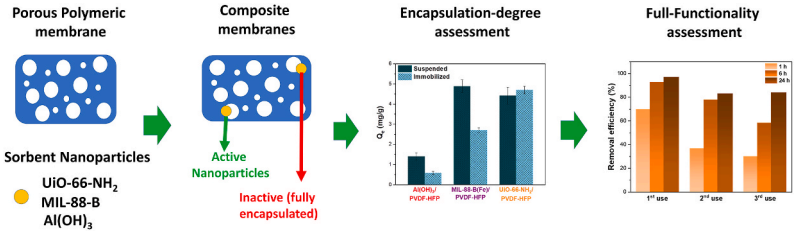

ARTICLE INFO

Handling Editor: Xiangru Zhang

Keywords:
Adsorption
Chromium
Composite membrane
Metal-organic frameworks
Water remediation

ABSTRACT

Natural or industrial hexavalent chromium water pollution continues to be a worldwide unresolved threat. Today, there is intense research on new active and cost-effective sorbents for Cr(VI), but most still exhibit a critical limitation: their powdered nature makes their recovery from water cost and energy consuming. In this work, $Al(OH)_3$, MIL-88-B(Fe), and UiO-66-NH_2 Cr(VI) sorbents were immobilized into a poly (vinylidene fluoride-co-hexafluoropropylene) (PVDF-HFP) polymeric substrate to develop an easily reactivable and reusable water filtering technology. The immobilization of the sorbents into the PVDF-HFP porous matrix modified the macro and meso-porous structure of the polymeric matrix, tuning in parallel its wettability. Although a partial blocking of the Cr(VI) adsorptive capacity was observed for of $Al(OH)_3$ and MIL-88-B(Fe) when immobilized into composite membranes, PVDF-HFP/UiO-66-NH_2 filter (i) exceeded the full capacity of the non-immobilized sorbent to trap Cr (VI), (ii) could be reactivated and reusable, and (iii) it was fully functional when applied in real water effluents.

* Corresponding author.
** Corresponding author.
E-mail addresses: roberto.fernandez@bcmaterials.net (R. Fernández de Luis), pamartins@fisica.uminho.pt (P.M. Martins).
[1] These authors equally contributed to this work.

https://doi.org/10.1016/j.chemosphere.2022.135922
Received 21 April 2022; Received in revised form 29 July 2022; Accepted 30 July 2022
Available online 5 August 2022

1. Introduction

Achieving a zero toxic water environment is one of the main challenges of the XXI century. Nowadays, more than 1.5 million deaths are estimated to be directly or indirectly related to health problems arising from water pollution (WHO/UNICEF, 2019; Langford, 2005; Fisher, 2018). Indeed, more than 80% of the wastewater released into the environment lacks the appropriate treatment to mitigate pollution, as is the case of Cr(VI) derived from metal plating, leather tanning, or mining (Bakshi and Panigrahi, 2018; Li et al., 2021). The environmental and health risks arising from chromium are closely related to its oxidation state. For instance, the toxicity, bio-persistence, carcinogenicity, and environmental mobility of Cr(VI) are significantly higher than the ones of Cr(III) (Speer and Wise, 2018). As a result, Cr(VI) is considered by the Environmental Protection Agencies one of the top-priority hazardous contaminants (Murad et al., 2022a).

Cr(VI) removal from water is faced from different technological perspectives, such as co-precipitation (Gopalratnam et al., 1988), reverse osmosis (Slater et al., 1983), ion exchange (Kim and Benjamin, 2004), membrane filtration (Efome et al., 2018), coagulation (Bora and Dutta, 2019), and flocculation (Sun et al., 2020). Having each technical approach its pros and cons, all of them show similar Achilles' Neels: high operating costs, pH sensitivity, and in particular, the lack of efficiency to lower Cr(VI) concentrations below the legal thresholds under certain operation conditions (Hu et al., 2004). These technical limitations are closely linked to Cr(VI) speciation as highly soluble and mobile chromate $(H_xCrO_4)^{-2+x}$ and dichromate $(Cr_2O_7)^{2-}$ oxyanions.

In this context, specific adsorption is considered one of the greener alternative to tackle Cr(VI) water pollution. Sorbents should be highly selective and efficient, easy to process, maintain and apply, do not require, or induce the addition or generation of secondary chemicals, and have a low cost (Fiyadh et al., 2019; Pavithra et al., 2019; Zhu et al., 2021). Ideally, an efficient and fast adsorption is closely linked to the density and affinity of the adsorbent's specific sites for Cr(VI) anions (Wadhawan et al., 2020). A variety of carbon-based (Hashemi and Rezania, 2019), metal oxides (Valentín-Reyes et al., 2019), clays and zeolites (Ghani et al., 2020) and, more recently, metal-organic framework (MOF) materials (Far et al., 2020; Mahmoud et al., 2022; Fang et al., 2018; Daradmare et al., 2021) have been applied to efficiently capture Cr(VI) from polluted ideal or real water matrixes (Nasrollahpour and Moradi, 2017; Wu et al., 2018a; Gao et al., 2021; Zhang et al., 2021; Zhou et al., 2021). Nevertheless, the main drawback that hinders the powdered sorbents' real applicability is their time and energy-consuming recovery (i.e. most usually by centrifugation or magnetic- based) from the water media once saturated (Wadhawan et al., 2020).

The immobilization of the active materials into polymeric substrates stands out as one of the most appealing strategies to solve this handicap. Polymeric composites bring the opportunity to merge the functions of the sorbents with the easy manipulation of filtering or membrane technologies (Choi et al., 2014). The variety of possible polymers and sorbents combinations (Gupta et al., 2021; Zhang et al., 2021), and the control over the final macro to micro pore-structure of the composite membranes, open up the perspective to obtain easily recoverable, reactivable, and function/pollutant-tailored technologies for water remediation purposes (Ng et al., 2013; Salazar et al., 2016; Martins et al., 2019a; Grandcolas and Lind, 2022; Vinothkumar et al., 2022). In this scope, poly (vinylidene fluoride-co-hexafluoropropylene), PVDF-HFP, stands out compared to other polymeric materials because of its mechanical, thermal, and chemical stability, simplicity of processability, and precise control over its porous structure when manufactured by different means. Indeed, among the scarce research on PVDF-HFP for environmental purposes, PVDF-HFP composite membranes have proven their efficiency to capture and separate both inorganic and organic pollutants (Salazar et al., 2016, 2022; Zioui et al., 2020; Martins et al., 2022).

In this work, the potential of water filtering technologies based on sorbent/PVDF-HFP composite membranes has been studied for the specific case of hexavalent chromium. It is demonstrated that PVDF-HFP based composite membranes (CM) immobilize the active sorbents homogeneously, and in parallel, the sorbent particles themselves induce a templating effect on the porous structure of the PVDF-HFP matrix as well. The adsorption capacity, efficiency, and kinetics of the non-immobilized sorbents and of the PVDF-HFP/Sorbent membranes have been investigated.

2. Experimental

2.1. Composite membranes preparation

Three different composite membranes ($Al(OH)_3$/PVDF-HFP, UiO-66-NH_2/PVDF-HFP, and MIL-88-B(Fe)/PVDF-HFP) were prepared following the general guidelines provided in (Salazar et al., 2016; Aoudjit et al., 2021). In short, a 10 wt % of sorbents were dispersed under ultrasonication in DMF for 3 h until a complete dispersion of particles was obtained (Salazar et al., 2020, 2021; Martins et al., 2022). This sorbent loading is selected to achieve the best compromise between the efficiency and the mechanical stability of CMs. Afterwards, PVDF-HFP was added (15:85 v/v), and the dispersion was magnetically stirred until the complete dissolution of the polymer. Then, the solution was spread on a glass substrate using a doctor blade and air-dried at room temperature for about 4 days. Membranes with 250 μm thickness were obtained after the process.

2.2. Samples characterization methods

The sorbent and composite membranes were fully characterized by means of X-ray diffraction, scanning electron microscopy, surface area measurements, mercury intrusion porosimetry, contact angle, thermogravimetric and differential scanning calorimetric measurements, and infrared spectroscopy. A detailed description of the measurement conditions and samples preparation can be found in the supplementary information file.

2.3. Chromium adsorption evaluation

Quantification of Cr(VI) in all kinetic and adsorption isotherm experiments was performed through UV–Vis spectroscopy (Tecan Infinite M Nano + spectrophotometer) by applying the previously reported diphenyl carbazide (DFC) colorimetric methodology (Saiz et al., 2020a; G. Saiz et al., 2021). For powdered sorbents, adsorption experiments were conducted at room temperature, using 10 mg of material dispersed in 10 mL of a 5 mg/L Cr(VI) solution. The dispersions were magnetically stirred for 24 h, and aliquots were withdrawn at defined time intervals. Afterwards, the aliquots were centrifuged at 6000 rpm for 10 min, filtrated with a hydrophilic 0.20 μm filter, and analyzed by the DFC protocol. Adsorption experiments with the composite membranes were performed following the same batch mode procedure, using a 100 mg mass of CM (i.e., 10 mg of active sorbent material immobilized within the composite) placed in the bottom of a beaker with 10 mL of a 5 mg/L Cr(VI) solution. The isotherm curves were obtained by obtaining the equilibrium adsorption capacity of the CM for Cr(VI) solutions of increasing concentrations. The performance of the UiO-66-NH_2/PVDF-HFP composite membrane was tested as well using a water sample from *Cávado River* (Barcelos, Portugal) as a matrix to include a controlled concentration of Cr(VI) ions. The physicochemical properties of this real sample are provided in Table S1.

Chromium adsorption efficiency (E) and capacity (Q_e) were evaluated according to Equations S1 and S2. The kinetic curves were fitted according to nonlinear forms of pseudo-first-order (Aggarwal et al., 2022), pseudo-second-order (Zhou et al., 2022), Elovich (Priya et al., 2022), and Bangham (Singh et al., 2021) kinetic models, expressed in

Equations S3 to S6 (Supporting Information), respectively. The adsorption isotherms were fitted according to Langmuir (Murad et al., 2022b), Freundlich (Mao et al., 2021), Temkin (Priya et al., 2022), and Dubinin-Radushkevich (Ammar et al., 2021) models, which are described by Equations S7 to S11 (Supporting Information), respectively.

3. Results and discussion

3.1. Sorbents characterization

The sorbents were selected on the basis of the simplicity of their synthesis, the characteristics of their surface chemistry and charge, and surface or inner porosity. Metal-Organic Frameworks (MOFs), metal oxides and zeolite particles were pre-selected as potential sorbents to test their affinity to capture Cr(VI) oxyanions before and after their immobilization into polymeric matrices (Renu et al., 2016). All the selected materials can be acquired commercially. However, the MOFs have been synthesized under specific conditions (see experimental section), to control their defect chemistry, crystallinity, and porosity.

SEM was initially employed to evaluate the morphology and particle size distribution for the sorbents (Figure S1 a). $Al(OH)_3$ and Fe_3O_4 presented irregular shaped morphologies with average sizes of 701 ± 320 nm and 959 ± 802 nm, respectively. The particle size values differed significantly from the ones provided by commercial description of the samples (Souza et al., 2015; Shen et al., 2016). This fact could be attributed to some degree of agglomeration during the preparation of the samples for the SEM observations. MOF samples exhibited aggregate morphologies as well. From the SEM images, individual particle diameters close to 200 nm could be estimated for MIL-125 and UiO-66-NH_2. Both MOFs shown broad particle diameter distribution accounting for individual crystals and aggregates of average size of 489 ± 225 nm for MIL-125 and 634 ± 302 nm for UiO-66-NH_2. In the specific case of MIL-88-B(Fe) and NanoNaY, the samples were formed by micro-meter size single-crystals with octahedral morphologies with average diameters of 1350 ± 66 nm and 1752 ± 809 nm, respectively.

XRD data was applied to confirm the purity and crystallinity of the materials. The comparison of the experimental and simulated powder XRD patterns (Figure S2) confirmed that the diffraction fingerprint of the sorbents matches the expected theoretical one. $Al(OH)_3$ exhibited the crystalline structure of bayerite aluminum hydroxide polymorph (Salazar et al., 2016). Fe_3O_4 had the characteristics pattern for the magnetite iron oxide cubic spinel like structure (Masudi et al., 2020). Then diffraction peaks of NanoNaY could be attributed to the crystalline planes of the cubic structure of NaY zeolite (Salazar et al., 2015). Similarly, the XRD pattern of MIL-125 and UiO-66-NH_2 were in agreement with the data reported in previous studies (G. Saiz et al., 2021; Saiz et al., 2020a). In the specific case of MIL-88-B(Fe), the XRD data pointed that the compound is the characteristics closed form of this MOF with a flexible framework (Hou et al., 2018). In addition, the pattern matching analyses of the XRD data for all the samples discard the presence of minor impurities (Salazar et al., 2015; Salazar et al., 2016; Hou et al., 2018; Masudi et al., 2020; Saiz et al., 2020a; G. Saiz et al., 2021).

The sorbents were characterized by FTIR to identify the chemical functions that could participate into the chromate anions adsorption (Figure S3). Among the multiple IR characteristic peaks, it is important to highlight the infrared (IR) absorption bands at ≈ 3410, 3470, 3550, and 3655 cm^{-1}, related with the vibrational modes of hydroxyl groups of bayerite sample (Salazar et al., 2016). For MOF samples, the FTIR spectra mainly contained the vibrational modes related to the symmetric and asymmetric vibration of C–O carboxyl group (≈1400, 1535 and 1685 cm^{-1}) and N–H deformation of the organic linkers (Castellanos et al., 2019; Rahmani and Rahmani, 2020). For UiO-66-NH_2, an additional weak band has been identified at approximately 1700 cm^{-1}. This fingerprint signal is associated with the stretching vibrational modes of C═O groups belonging to the uncoordinated positions arising from the amino-terephthalate linkers, that is, to defective position within the framework of the UiO-66-NH_2. For instance, it has been demonstrated that incorporating hard modulators (i.e., HCl) in the synthesis media induces a certain degree of linker defects within the material, which benefits the adsorption of anionic species as Cr(VI) anionic species (Saiz et al., 2020a).

TGA analyses were also performed for the MOF samples (Figure S4). MIL-125 and MIL-88-B(Fe) show a two-stage thermal degradation: (i) dehydration process (30–125 °C), and (ii) organic linker calcination (250 °C for MIL-88-B and 325 °C for MIL-125 samples) (Golmohamadpour et al., 2018). For the UiO-66-NH_2 sample, a three-stage degradation was observed: (i) solvent release (30–125 °C), (ii) cluster dehydration (150–300 °C) and (iii) linker calcination (325–400 °C). As explained in detail by Saiz et al. (2020a) and G. Saiz et al. (2021), the linker defect degree within the UiO-66-NH_2 material can be estimated based on the thermogravimetric normalized weight loss associated with the organic linkers' calcination. Based on this calculation, 0.5 linker defects per zirconium hexa-nuclear clusters could be estimated.

Dynamic light scattering, and zeta potential measurements were performed for the specific case of UiO-66-NH_2 in order to assess the hydrodynamic size distribution and the periphery surface charge of the sample (Figure S5). In agreement with the conclusions drawn by SEM analyses, dynamic light scattering data pointed out to a bimodal distribution of the UiO-66-NH_2 particle size with average diameters of 150 and 600 nm (Figure S5 a). In addition, the zeta potential values of the UiO-66-NH_2 dispersions in water indicated a zero-charge point located at a pH close to 4, above which the UiO-66-NH_2 particles exhibited negative surface potential values up to −40 mV at pH 11 (Figure S5 b). The protonation of the amino groups within the UiO-66-NH_2 framework explains the positive values of the zeta potential below a pH 4, while the negative surface charge at higher pH values can be ascribed to the hydroxyl groups at the surface uncoordinated positions of the UiO-66-NH_2 particles (Ibrahim et al., 2019).

3.2. Functional characterization of the sorbents

An initial assessment of the capacity of the sorbents to capture Cr(VI) was performed in order to identify the best candidates to be immobilized within the PVDF-HFP membranes. Punctual adsorption experiments over a high concentrated 100 mg/L Cr(VI) solution were carried out as a probe test. The UV–Vis quantification of the Cr(VI) concentration before and after the adsorption process allows estimating the Cr(VI) removal efficiency for each material, as shown in Fig. 2 (a). As evidenced by these initial results, MIL-88-B(Fe), UiO-66-NH_2 and $Al(OH)_3$ stood out as the best of the selected materials to capture Cr(VI). Given the high concentration of the initial chromium solution, the adsorption capacity values were foreseen to be close to the maximum expected ones for each material, as supported by previously investigations (Salazar et al., 2016; Niu et al., 2017; Wu et al., 2018b). The difference in the adsorption capacities obtained for each material can be explained on the basis of the different chromium immobilization mechanisms for each sorbent. Cationic NanoNaY zeolite lacks the capacity to retain negative chromate ions (Lopes et al., 2012). Iron-based materials (i.e., Fe_3O_4 and MIL-88-B (Fe)) combine the iron affinity over the capture of chromium with the iron-based Fenton-mechanism to reduce Cr(VI) to Cr(III). Bayerite retain chromate by anionic exchange with the hydroxyl surface groups. As reported previously, UiO-66-NH_2 possesses a threefold chromium immobilization mechanism: chemisorption at the inorganic clusters, electrostatic sorption at the amino protonated groups, and reduction to trivalent chromium at the same positions (Zango et al., 2019; Saiz et al., 2020a).

3.3. Composite membranes characterization

Based on the initial Cr(VI) adsorption tests, $Al(OH)_3$, MIL-88-B(Fe), and UiO-66-NH_2 were selected to assemble 10 wt % sorbent/PVDF-

HFP CMs. The sorbent loading was selected considering our previous investigations to reach a compromise between the performance of CM and its mechanical and chemical stability (Salazar et al., 2020, 2021; Martins et al., 2022). After assembling the CM by solvent casting (i.e., as detailed in the experimental section and in the supporting information file), the morphological, chemical, spectroscopic, and thermal characterization of the CMs was performed to evaluate whether the sorbents were fully or partially functional after their immobilization into the polymeric matrix. That is, if the specific placement within the macro to mesoporous structure or the PVDF-HFP matrix modulated its capacity to capture chromium anions.

Surface and cross-section SEM images (Fig. 1 a–d) indicate that the slow evaporation of the solvent promoted the formation of a micrometric well-distributed porous structure for all composite membranes (Ribeiro et al., 2018). For the pristine PVDF-HFP, a homogeneous spherulitic morphology (0.4–2.6 μm) with a well-defined and interconnected pore structure was formed. Noticeable, the immobilization of different sorbents did not significantly affect the PVDF-HFP matrix structuration at the micrometer scale (Fig. 1 b–d). Nonetheless, a slight modification of surface morphology was observed. Indeed, the average diameter of the spherulites in the PVDF-HFP sample was 1.96 ± 0.61 μm (Min.: 0.87 μm, Max.: 4.5 μm) (Figure S6 a). A perfect cubic or close hexagonal packing of 2 μm spherulites would lead to pores with diameters equal or below 1 μm, which was the value where the maximum pore diameter distribution of the PVDF-HFP was located, as observed in mercury porosity measurements discussed in the following (Fig. 1g and S6 b–c). As a significant dispersion of the spherulites diameter was observed, the pores arising from their packing can slightly exceed this range but did not justify the existence of pores with diameters far above 1 μm. This porous structure was predicted by the phase diagram of the PVDF-HFP and the binary system of DMF, in which areas of miscibility and phase separation are noted (Ribeiro et al., 2018). Additionally, the interconnectivity of the pores shape percolation pathways for water across the membranes that connected the immobilized active materials, as long as they were not fully encapsulated within the PVDF-HFP matrix (Teixeira et al., 2016).

XRD patterns of the CMs confirmed the presence of the sorbents after their incorporation within the PVDF-HFP matrix. The slight differences in the positions of the diffraction peaks of the MIL-88-B(Fe) sample after its immobilization in the polymer can be explained by the flexible structural nature of this material (Zango et al., 2019). As the MIL-88-B (Fe) structure responded to the solvent loading, a slight displacement of the diffraction maxima was predictable in comparison to the activate sample studied within the first section of this work.

FTIR spectroscopy further confirmed the immobilization of the sorbents within the CM and given access to identify the polymeric phases of PVDF-HFP (Fig. 1 e). FTIR spectra of PVDF-HFP exhibited the characteristic absorption bands of C(F)–C(H)–C(F) skeletal bending, C–C and F–C–F symmetrical stretching, and C–F stretching at 875, 1072, 1169, and 1404 cm^{-1}, respectively. It was noted that the immobilization of inorganic $Al(OH)_3$ did not result in additional bands in the FTIR spectra of CMs. For the specific case of MOF-based membranes, three weak additional signals, associated to the vibrational modes of the organic linkers, were observed at 747, 1598, and 1659 cm^{-1} were observed (Zango et al., 2019).

The DSC curves of PVDF-HFP composite membranes (Fig. 1 f) confirmed the characteristic endothermic melting of the polymer crystalline phase at 142 °C followed by the thermal degradation of the polymer (Ribeiro et al., 2018); two characteristic parameters of the PVDF matrix that were not significantly affected by the presence of the sorbent materials (Ribeiro et al., 2018). The TGA profiles of the composite membranes shown an additional endothermic step related to the dehydration process of the MOFs. (Figure S7).

Mercury porosimetry measurements for the polymeric and

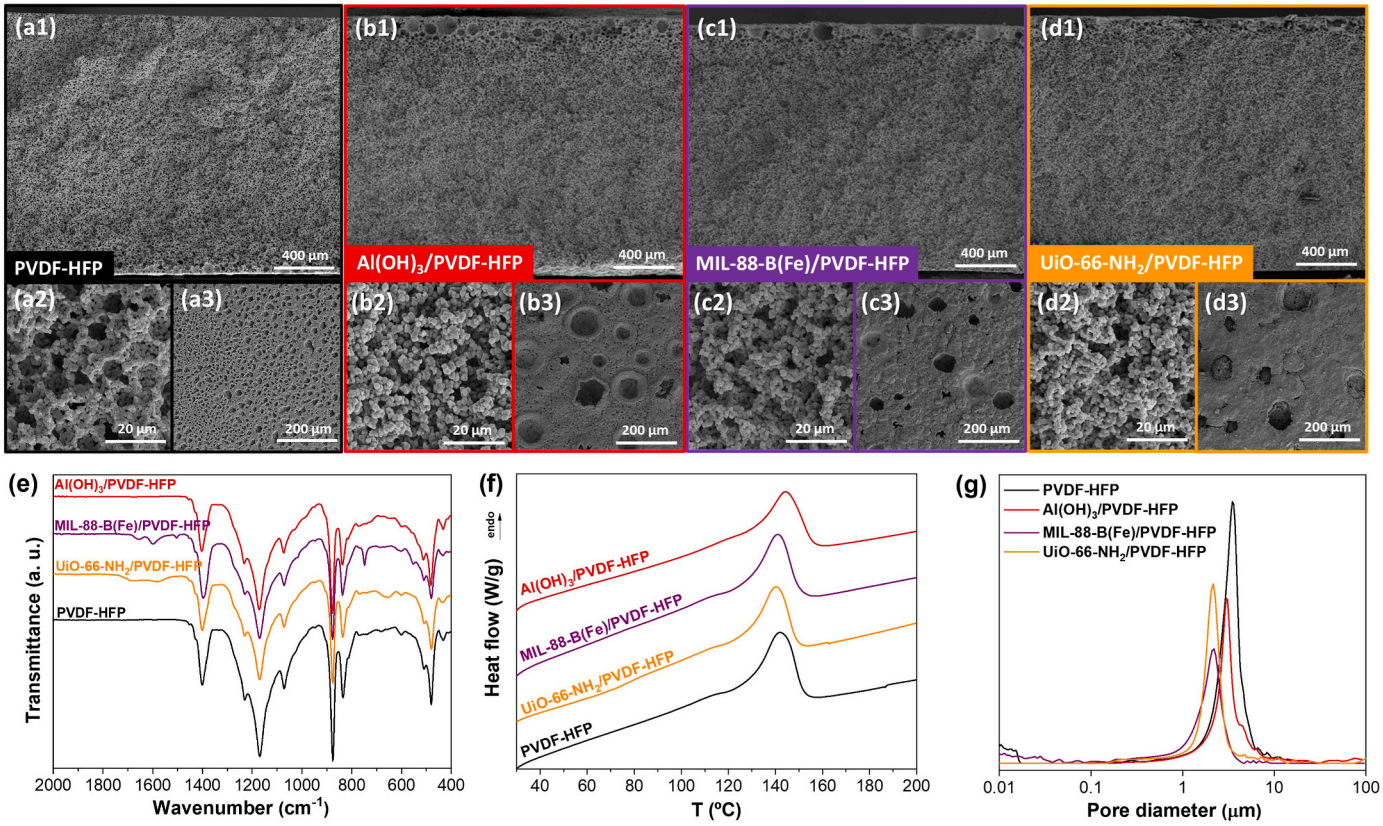

Fig. 1. **(a–d)** Representative SEM images, **(e)** FTIR spectra, **(f)** DSC curves, and **(g)** porosimetry measurements of $Al(OH)_3$/PVDF-HFP, MIL-88-B(Fe)/PVDF-HFP, and UiO-66-NH_2/PVDF-HFP composite membranes.

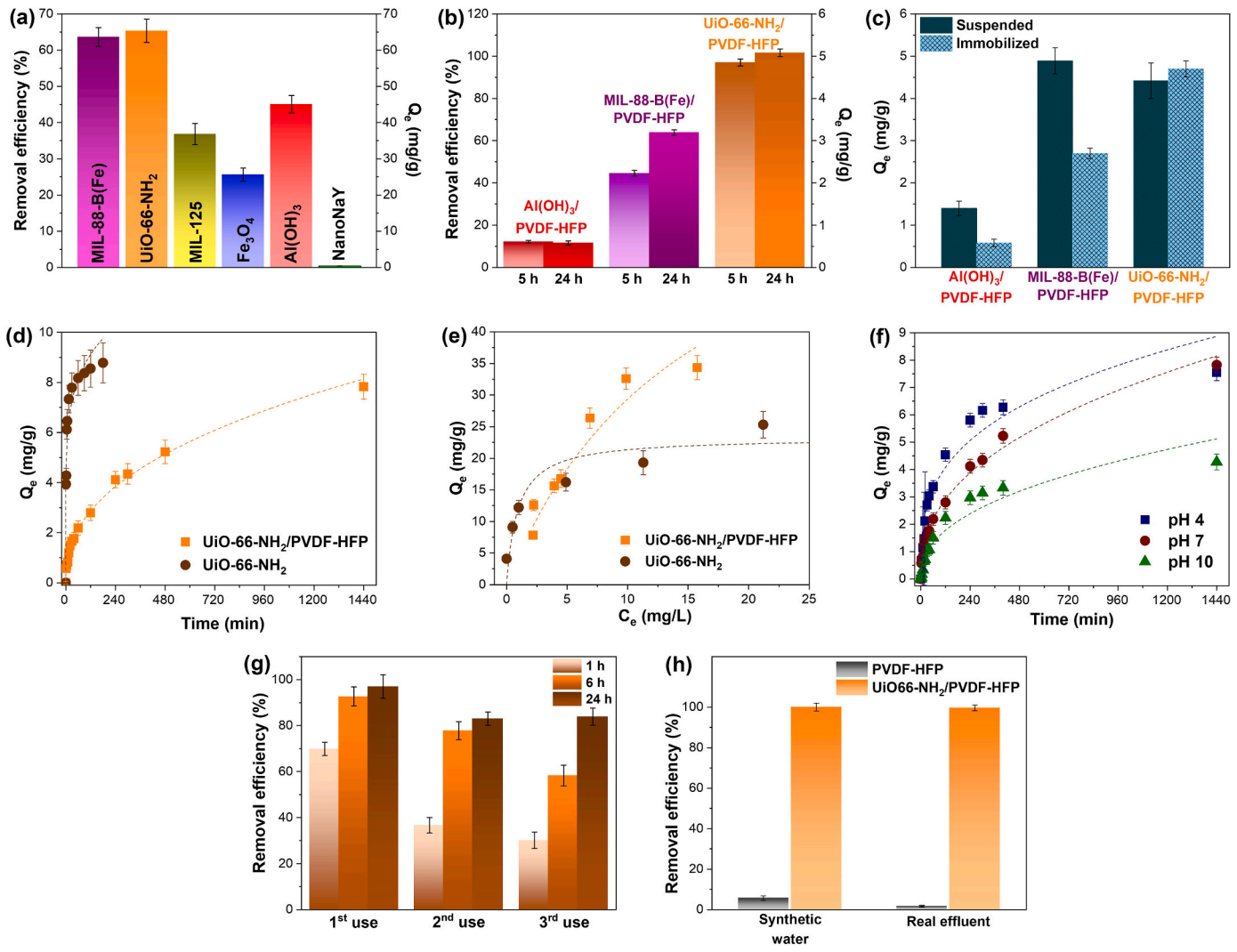

Fig. 2. Cr(VI) adsorption efficiency and capacity of (a) sorbents (dosage: 1 g/L; [Cr(VI)] = 100 mg/L; t = 60 min); and (b) composite membranes; **(c)** comparison of adsorption capacity of suspended and immobilized $Al(OH)_3$, MIL-88-B(Fe), and UiO-66-NH_2 sorbents ([Cr] = 5 mg/L, pH = 7, t = 24 h, dosage: 1 g/L); **(d)** Kinetic curve of Cr(VI) adsorption fitted with the model ([Cr] = 5 mg/L; pH = 7; t = 24 h), and **(e)** Cr(VI) adsorption isotherm fitted to Langmuir model (pH = 7; t = 24 h); **(f)** effect of pH on Cr(VI) removal by UiO-66-NH_2/PVDF-HFP ([Cr] = 5 mg/L; t = 24 h); **(g)** reusability of the CM ([Cr] = 5 mg/L; pH = 7; equilibrium time = 24 h), and **(h)** Cr(VI) removal experiment on real water matrix ([Cr] = 5 mg/L; pH = 7.7; time = 24 h; the contribution of PVDF-HFP matrix has been subtracted).

composite membranes given access to quantify the pore volume distribution (Fig. 1 g). Most of the empty volume of the solvent casting processed PVDF-HFP lied within 2 and 6.5 μm pores, with a maximum of the pore volume associated to an average pore diameter of 3.5 μm. The inclusion of the sorbents induced a decrease of the pore's diameter and a narrowing of the pore size distribution in comparison to pristine PVDF-HFP (i.e., Bayerite: 3.5 μm, (Min: 2 μm and Max: 6.5 μm), MIL-88: 2.15 μm (Min: 0.7 and Max: 4.5 μm) and UiO-66-NH_2: 2.15 μm, (Min: 1.2 and Max: 4.5 μm)). Overall, an increase of the total porosity and surface areas has been observed for composite membranes compared to the pristine polymer (Table S3). Thus, it is important to mention that the information obtained from mercury porosimetry and electron scanning microscopy is complementary since mercury intrusion within the membranes gives access to uncover which pores observed by SEM accounts for the larger fraction of the surface area of the membranes.

Contact angle measurements (Figure S8) corroborated the hydrophobic nature of the porous PVDF-HFP membrane (Ribeiro et al., 2018) with a contact angle of 165°. In comparison, composite membranes exhibited an important improvement of their wettability, with a marked hydrophilic nature (contact angle of 0°). The surface morphology and chemistry can partially explain the modification of the wetting behavior. Nonetheless, it is important to consider the composite membranes' topography and surface roughness as important parameter that promote the water permeability as well (Correia et al., 2019; Martins et al., 2019b).

3.4. Functional characterization of composite membranes

The punctual adsorption efficiency and capacity of the CMs were evaluated under 5 mg/L hexavalent chromium solutions (Fig. 2 b and Table S4). A PVDF-HFP membrane was employed as a control. As expected, it possessed a near negligible capacity to retain Cr(VI) (5.7% removal and Q_e = 0.14 mg/g). Opposite, CMs offered higher efficiencies to retain chromate anions, with 12, 62 and 97% of chromium removal after adsorption for $Al(OH)_3$/PVDF-HFP (Q_e = 5 mg/g), MIL-88-B(Fe)/PVDF-HFP (Q_e = 3 mg/g), and UiO-66-NH_2/PVDF-HFP (Q_e = 3 mg/g), respectively.

Conventional characterization techniques do not give access to unravel the complete picture of the CM structures, such as the active materials' inactivation due to their full encapsulation within the polymeric host. Therefore, one of the primary goals of this work was to assess whether indirect approaches, as the comparison of the adsorption

kinetics or isotherms of the active materials and of the PVDF-HFP-based CM, could help us to estimate this parameter as well. The Cr(VI) adsorption capacity of the active materials immobilized on the membranes has been calculated considering the weight of the CM, the 10 wt % loading of the sorbents, and the volume and concentration of the Cr (VI) solution. The contribution of the PVDF-HFP matrix to the adsorption (i.e., ≈6%) has been subtracted to obtain a more accurate value. In parallel, the adsorption capacity of the suspended sorbents was obtained in the same experimental conditions. The data has been plotted and summarized in the Fig. 2 (c) and Table S4. When comparing the adsorption capacity of the active sorbent materials before and after their immobilization into the PVDF-HFP matrix (Fig. 2c), it is clear that there was a significant reduction of the capacity for $Al(OH)_3$ and MIL-88-B (Fe). In contracts, the adsorption capacity of UiO-66-NH_2 adsorption capacity remained constant after its incorporation within the PVDF-HFP membrane. Therefore, chromium adsorption experiments given us an indirect clue to estimate that the encapsulation of UiO-66-NH_2 particles is almost negligible, while the 65 and 45% of the $Al(OH)_3$ and MIL-88-(B) particles were somehow embedded within the polymeric matrix losing their functionality.

Since the UiO-66-NH_2/PVDF-HFP composite was the most promising one of the studied, we continued its functional characterization in order to fully understand the kinetics (Fig. 2 (d)) and adsorption capacity (Fig. 2e) of the active material immobilized within the PVDF-HFP in comparison to the non-immobilized material (Hamoudi et al., 2018; Saiz et al., 2020a). First, adsorption kinetics of UiO-66-NH_2/PVDF-HFP was significantly lower than the one of the suspended UiO-66-NH_2 sorbent. Even though, the 50% of the chromium uptake occurred within the first 4 h of the experiment. This finding is related to the lower mass transfer across the PVDF-HFP matrix. Pseudo-first order, pseudo-second order, Elovich, and Bangham kinetic models were used to fit the experimental data. The parameters obtained from the fittings have been summarized in Figure S9 and Table S5. The Bangham's fittings for the sorbent and the composite membrane have been plotted as dotted lines in the Fig. 2 (d). Bangham and pseudo-second order models were the ones that match better with the experimental data of the composite membrane, as both present the smallest RMSE values. The figures of merits obtained from the fitting with the Bangham kinetic model suggested that adsorption was mainly governed by intraparticle diffusion phenomena (Edet and Ifelebuegu, 2020; G. Saiz et al., 2021). In parallel, the pseudo-second-order kinetic model indicated that Cr(VI) removal by CM was not merely governed by diffusion, but chemisorption also occurred during adsorption (Choong et al., 2021). Both conclusions agree with the nature of our composites since the PVDF-HFP matrix imposes diffusion limitations to the chromium anions to reach the UiO-66-NH_2 particles, whilst Cr(VI) chemisorption occurs at the microporous structure of the UiO-66-NH_2.

The Cr(VI) adsorption capacity of the CM and the active material was assessed (Table S6). In agreement with the kinetic studies, the adsorption capacity of the sorbent was maintained after its immobilization, with a Q_{max} value of 59.9 mg/g. However, the profile of the isotherms differed significantly for the non-immobilized and the immobilized material. For instance, the adsorption capacity at low concentrations was higher for the non-immobilized UiO-66-NH_2 but was reversed in the higher Cr(VI) concentration range for the active material immobilized in the composite membrane. Although the explanation to these experimental evidence it is still unclear, this tendency suggests that the PVDF-HFP play an active role in the composite membranes for the Cr(VI) absorption at high concentrations. (Guo et al., 2021; Zhang et al., 2022). Based on the experimental data, adsorption isotherms were fitted using Langmuir, Freundlich, Temkin, and Dubinin-Radushkevich models (Figure S10 and Table S7). The RMSE value for Langmuir fitting was slightly inferior to the remaining models both for the free and immobilized material (Fig. 2 e). Langmuir model assumes that the adsorption process takes place on a homogeneous surface with adsorption sites of similar affinity for Cr(VI), so a monolayer of adsorbate Cr(VI) oxyanions is formed on UiO-66-NH2 pore space of the composite membranes (Bilgiç and Çimen, 2019). Langmuir adsorption equilibrium constant accounts for the affinity of the sorbent for the adsorbate, so the inclusion of the UiO-66-NH_2/PVDF-HFP CM exhibited a lower overall adsorption affinity over chromium in comparison to the active materials because the PVDF-HFP matrix hindered the migration of chromium anions to the active adsorption sites of UiO-66-NH_2.

As chromium speciation was highly dependent on the pH of the media (Figure S11, (Dvoynenko et al., 2021)), the dependence on the adsorption affinity of the composite membranes was studied also in function of this parameter. (Fig. 2 (f) and Table S8). On the other hand, the surface chemistry, and the protonation degree on the amino groups of UiO-66-NH_2 was highly dependent on the pH, increasing as the acidity pH the media did.

It was thus observed that Cr(VI) adsorption by UiO-66-NH_2/PVDF-HFP was affected by the pH of the media similarly as the active material did. Previous research has proved the overperformance of Zr-based MOF materials to capture Cr(VI) at acidic conditions compared to neutral or basic ones (Ibrahim et al., 2019). Similarly, acidic, and neutral environments proved to be the most favorable for efficient adsorption of the developed composite membranes, whilst the adsorption process was significantly affected under alkaline conditions. The adsorption kinetics were faster under acidic conditions as well. As in all the explored conditions, the chromate was stabilized as negative species, the adsorption dependence on the membrane could be explained based on the UiO-66-NH_2 increasingly protonation - as the acidity of the media increased. When the pH value was nine, the amino groups were mostly in their neutral form, and all the chromate adsorption was foreseen to be ascribed to its chemisorption at the zirconium hexanuclear clusters of the UiO-66-NH_2 framework. Opposite, as the acidity of the media increased, the protonation degree of amino groups did, promoting the chromium uptake through $NH_3^+\cdots Cr(VI)^{n-}$ electrostatic interaction. However, as demonstrated by Saiz et al. (2020a), the capture of hexavalent chromium species by Zr-MOFs is far to be a single adsorption process since a partial reduction of Cr(VI) to Cr(V) and Cr(III) is promoted as a consequence of the functional groups within the framework.

The reusability of the CM was evaluated by performing three consecutive uses. Between each use, the composite membrane was reactivated under magnetic stirring for 4 h with a 1 M HCl solution and further washed with ultra-pure water for 2 h. After the desorption process, a new Cr(VI) solution was placed in contact with the membrane to evaluate its performance. The results of reusability tests were shown in Fig. 2 (g), whilst the raw data were summarized in Table S9. The first conclusion drawn by the reusability tests was that the loss of the efficiency of the membranes was attenuated during consecutive regeneration and reuse cycles. For instance, the adsorption capacity fading was accentuated during the initial adsorption cycles while recovered as the system reached equilibrium after 24 h. There is a possible passivation of the Cr(VI) reduction/Cr(III) adsorption active sites on MOF particles after each regeneration process, causing a slight decrease on the reduction/adsorption capacity of CM. Therefore, the regeneration caused a slight reduction of the functionality of the composite membranes in terms of adsorption kinetics.

The selectivity and efficiency of UiO-66-NH_2/PVDF-HFP on a real treated effluent matrix were studied in order to test the selectivity of the membranes to extract the Cr(VI) in complex matrixes that contain background competing ions (Speer and Wise, 2018; Zinicovscaia et al., 2020; Rasheed et al., 2020; Mahmoud et al., 2021; Meena and Arai, 2016). To this end, 5 mg/L of Cr(VI) were added to the effluent sample to perform the experiment. In the specific case of the tested water matrix, nitrate was the anionic competitor in a higher concentration (6 mg/L). Similarly than chromate, nitrate was not a strong coordinating group, and it was foreseen to share the same adsorption sites within the UiO-66-NH_2 sorbent (Wu et al., 2018b). Even though the efficiency of the system was maintained in real water matrices since no appreciable differences were observed in adsorption efficiencies or capacity of the

composites from ideal to real aqueous media (Fig. 2 h).

3.5. Hexavalent chromium adsorption mechanisms

UiO-66-NH_2/PVDF-HFP was characterized by means of compositional EDX mapping, UV–Vis, XRD and FTIR techniques after adsorption in order to shed some light in the functional mechanisms of the system. To this end, UiO-66-NH_2/PVDF-HFP membranes were characterized before and after exposing them to a 50 mg/L Cr(VI) and 5 mg/L Cr(VI) solution for three cycles. It is important to note that for specific techniques as FTIR or EDX mapping, no significant differences were obtained when studying the CMs exposed to low concentrated Cr(VI) solutions (5 mg/L). Therefore, it was necessary to augment the chromium loading by increasing the concentration of the initial Cr(VI) solution up to 50 mg/L.

First, cross-section compositional mappings of the membranes were obtained by SEM-EDX (Figure S12 and Fig. 3 (a), respectively). As expected, carbon, fluorine, zirconium, and oxygen were identified as the main elements constituting the sample. Although a homogeneous distribution of the zirconium and oxygen content associated with the UiO-66-NH_2 particles were found in the membranes, a certain degree of agglomeration was also observed at the compositional maps. For the membranes tested at 5 mg/L Cr(VI) solution, it was not possible to map its chromium content, although some of the punctual EDX analysis demonstrated its presence in the membrane. After exposing UiO-66-NH_2/PVDF-HFP to a 50 mg/L Cr(VI) solution, the chromium distribution along the membrane coincided with the zirconium enriched areas, thus, with the locations of the UiO-66-NH_2 component. This evidence further indicated that the chromium uptake was mainly ascribed to the MOF particles. This technique allowed concluding that at least at a micrometer regime, the system did not show blind adsorption areas.

UV–Vis spectroscopy was employed to unravel qualitatively the chromium speciation once immobilized in the composite membrane. The bare membranes exhibited two strong absorption bands at 250 and 350 nm associated with the charge transfer bands related to the MOF material. After use, there was a significant gain of absorbance of the band located at 350 nm, directly associated with the typical orange color attributed to the chromate oxyanions (Fig. 3 b). In addition, a broad but clear fingerprint also appeared at 570 nm. For instance, this UV–Vis signature was associated with the spin-allowed d–d transitions of an octahedral-coordinated Cr^{3+}d7, 4A2g(F) → 4T1g(F) transition, which confirmed the presence of trivalent chromium stabilized within the membrane. Henceforth, once immobilized within the PVDF-HFP matrix, the immobilized UiO-66-NH_2 is still able to adsorb and chemical reduce the Cr(VI) to Cr(III), as the material does when is applied in as a powder suspended in an aqueous solution. XRD patterns (Fig. 3 c) pinpointed that the UiO-66-NH_2 crystallinity was maintained after three adsorption/activation cycles in a 5 mg/L Cr(VI) solution, while there was a substantial loss of crystallinity when the membrane is exposed to a 50 mg/L Cr(VI) solution. After three consecutive adsorption and regeneration cycles, the diffraction maxima ascribed to the UiO-66-NH_2 shown an insignificant intensity loss, so, the immobilization of the sorbent into the PVDF-HFP matrix conferred an extra protective function that delays the UiO-66-NH_2 chemical degradation during activation.

Taking into consideration all the results, an adsorption mechanism for the Cr(VI) uptake by composite membranes was proposed. First, it is important to note that the particles immobilized within the PVDF-matrix can be stabilized in three different locations: (i) First, the active materials can be placed at the surface of the interconnected macro to meso

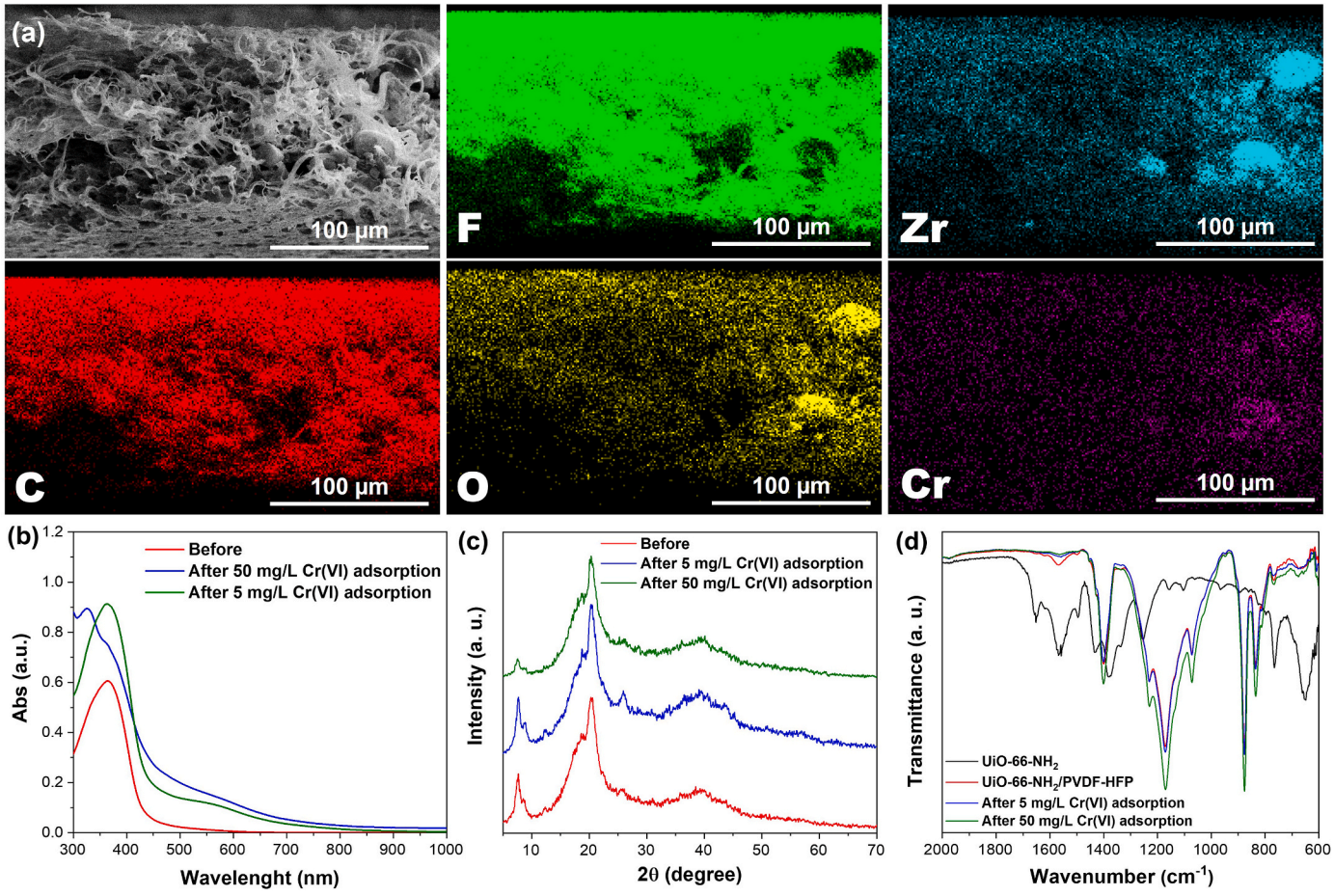

Fig. 3. **(a)** SEM-EDX mapping of CM before and after 50 mg/L Cr(VI) adsorption experiment; **(b)** UV–Vis spectra, **(c)** XRD patterns, and **(d)** FTIR spectra of CM before and after 5 mg/L and 50 mg/L Cr(VI) adsorption experiment.

pore-structure of the PVDF-HFP, and hence, being in a direct contact with chromium ions of the water solution (Fig. 4), (ii) the particle can migrate during the PVDF-HFP non-solvent induced phase separation to the surface of the isolated pores, or (iii) they can be encapsulated within the polymeric non-porous regions of the PVDF-HFP membrane (Fig. 4). In both last cases, the sorbents would be inactive for any adsorption function since the water solution would never reach these occluded areas of the membrane. For example, the adsorption capacity of the sorbent included within the $Al(OH)_3$/PVDF-HFP and MIL-88-B(Fe)/PVDF-HFP membranes was significantly lower than the one obtained for the experiments directly performed with the active materials. Therefore, it was foreseen that an important population of the $Al(OH)_3$ and MIL-88-B particles migrated to inactive positions within the PVDF-HFP matrix.

Opposite, the adsorption capacity of the UiO-66-NH_2 incorporated in the PVDF-HFP membrane was similar to the one of the non-immobilized material, suggesting that most of the UiO-66-NH_2 particles were placed at the surface of the interconnected pore structure of the PVDF-HFP matrix. These results suggested that the nature and properties of the sorbent may influence its migration during the NIPS process.

According to previous studies developed on MOF for chromium remediation from water, the adsorption process in the active material occurred through (1) electrostatic interactions between the NH_3^+ groups and negatively charged $[H_xCr(VI)O_4]^{-2+x}$ oxyanions; and (2) anionic exchange between the CrO_4^{2-} oxyanions and the OH^- groups linked to Zirconium hexanuclear clusters of the UiO-66-NH_2 framework (Fig. 4) (Saiz et al., 2020b; G. Saiz et al., 2021). Furthermore, the capacity of UiO-66-NH_2 to partially reduce Cr(VI) to Cr(III) species was also a point to consider. This mechanisms were also preserved in the PVDF-HFP composite membrane, as proved by the presence of the UV–Vis absorption band related to Cr(III) species after the Cr(VI) adsorption by UiO-66-NH_2/PVDF-HFP composite (Fig. 3 b). Surprisingly, the adsorption capacity Cr(VI) of UiO-66-NH_2/PVDF-HFP membrane overcome the average capacity of its individual components, an experimental result that pointed towards the existence of a synergistic effect between active material and the polymeric matrix. However, additional experimentation is needed to fully unravel the mechanisms at the interphase of the two materials that makes this extra-adsorption capacity possible.

4. Conclusions

The adsorption capacity of varied sorbents over hexavalent chromium (i.e. $Al(OH)_3$, Fe_3O_4, NanoNaY, MIL-125, MIL-88-B(Fe), and UiO-66-NH_2) was evaluated before and after their immobilization into PVDF-HFP polymeric composite membranes. These hybrid systems were fully characterized to gain a complete understanding of their porous structure from the macro to the micrometer scale.

All the studied membranes show a well-defined and interconnected micrometric porous structure and a hydrophilic nature. The Cr(VI) removal capacity of the active materials immobilized within the polymeric membranes points out that their partial or full functionality depends on their degree of encapsulation into the polymeric matrix, which in turn, depends on their intrinsic nature and surface characteristics.

UiO-66-NH_2/PVDF-HFP composite was the most effective in capturing chromium from simulated and real water samples with different acidities. A combination of intraparticle diffusion and chemisorption was identified as the most plausible mechanism to explain the adsorption kinetics of composite membranes. For instance, the membrane still exhibits the Cr(VI) to Cr(III) reduction capacity of the active UiO-66-NH_2 particles, which endow a dual adsorption/detoxification function to the membrane since Cr(III) species are much less environmentally hazardous than Cr(VI).

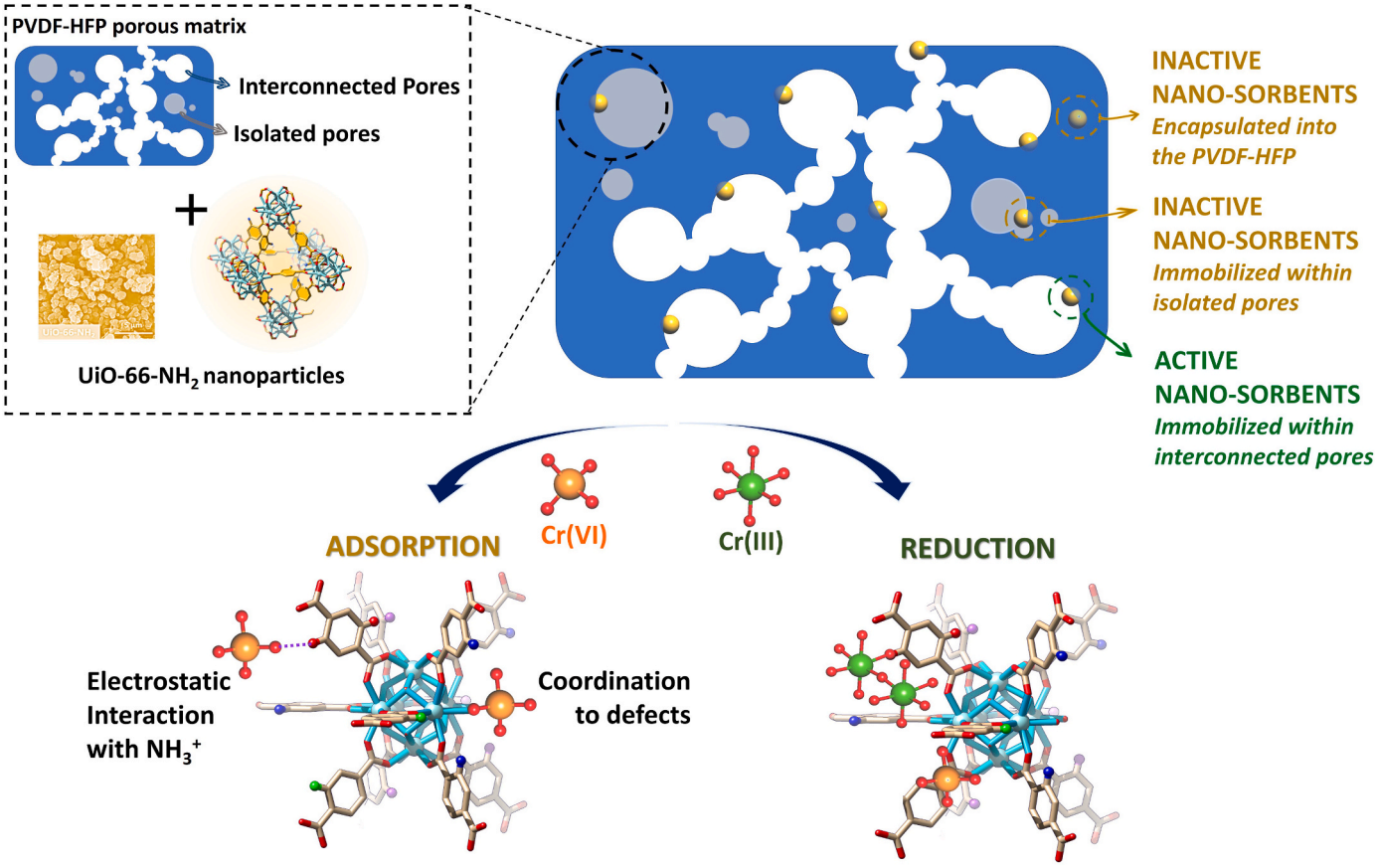

Fig. 4. Adsorption and reduction of Cr(VI) on UiO-66-NH_2/PVDF-HFP composite membrane surface.

Overall, the sorbent/PVDF-HFP composite technology is close to the capacity to capture Cr(VI) of the active materials in suspension, and in addition, it is easily recoverable, reactivable and reusable. The UiO-66-NH_2/PVDF-HFP composite membrane arises as to the most promising studied hybrid technologies to capture hexavalent chromium with outstanding efficiency, being functional under real water matrixes and different pH environments. Although there is still room for improvement to achieve a fast Cr(VI) adsorption kinetic by the hybrid membranes, this work poses the first step towards further developing an easily recoverable, reactivable and reusable technology for Cr(VI) removal from polluted industrial and mining acidic waters.

Author contributions statement

Joana M. Queirós: Conceptualization, Methodology, Software, Validation, Formal analysis, Investigation, Resources, Data Curation, Writing - Original Draft, Writing - Review & Editing, Visualization, Supervision, Project administration, Funding acquisition. **H. Salazar:** Conceptualization, Methodology, Software, Validation, Formal analysis, Investigation, Resources, Data Curation, Writing - Original Draft, Writing - Review & Editing, Visualization, Supervision, Project administration, Funding acquisition. **A. Valverde:** Conceptualization, Methodology, Software, Validation, Formal analysis, Investigation, Resources, Data Curation, Writing - Original Draft, Writing - Review & Editing, Visualization, Supervision, Project administration, Funding acquisition. **G. Botelho:** Conceptualization, Methodology, Software, Validation, Formal analysis, Investigation, Resources, Data Curation, Writing - Original Draft, Writing - Review & Editing, Visualization, Supervision, Project administration, Funding acquisition. **R. Fernández de Luis:** Conceptualization, Methodology, Software, Validation, Formal analysis, Investigation, Resources, Data Curation, Writing - Original Draft, Writing - Review & Editing, Visualization, Supervision, Project administration, Funding acquisition. **J. Teixeira:** Conceptualization, Methodology, Software, Validation, Formal analysis, Investigation, Resources, Data Curation, Writing - Original Draft, Writing - Review & Editing, Visualization, Supervision, Project administration, Funding acquisition. **P.M. Martins:** Conceptualization, Methodology, Software, Validation, Formal analysis, Investigation, Resources, Data Curation, Writing - Original Draft, Writing - Review & Editing, Visualization, Supervision, Project administration, Funding acquisition. **S. Lanceros-Mendez:** Conceptualization, Methodology, Software, Validation, Formal analysis, Investigation, Resources, Data Curation, Writing - Original Draft, Writing - Review & Editing, Visualization, Supervision, Project administration, Funding acquisition.

Declaration of competing interest

The authors declare that they have no known competing financial interests or personal relationships that could have appeared to influence the work reported in this paper.

Data availability

Data will be made available on request.

Acknowledgements

This work was supported by the Portuguese Foundation for Science and Technology (FCT) in the framework of the Strategic Projects UIDB/04650/2020 and UID/QUI/50006/2019 and project PTDC/FIS-MAC/28157/2017. H. Salazar and P.M. Martins thanks the FCT for grants SFRH/BD/122373/2016 and COVID/BD/151786/2021, and contract 2020.02802.CEECIND. Financial support from the Basque Government Industry and Education Departments under the ELKARTEK program is also acknowledged. Ainara Valverde acknowledges the Basque Government (Education Department) for her PhD grant (PREB_2018_1_004). The European Commission Research & Innovation H2020-MSCA-RISE-2017 (Ref.: 778412) INDESMOF project is also acknowledged. The authors thank the technical and human support provided by SGIker (UPV/EHU).

Appendix A. Supplementary data

Supplementary data to this article can be found online at https://doi.org/10.1016/j.chemosphere.2022.135922.

References

Aggarwal, R., Saini, D., Sonkar, S.K., Sonker, A.K., Westman, G., 2022. Sunlight promoted removal of toxic hexavalent chromium by cellulose derived photoactive carbon dots. Chemosphere 287.
Ammar, N.S., Fathy, N.A., Ibrahim, H.S., Mousa, S.M., 2021. Micro-mesoporous modified activated carbon from corn husks for removal of hexavalent chromium ions. Appl. Water Sci. 11.
Aoudjit, L., Salazar, H., Zioui, D., Sebti, A., Martins, P.M., Lanceros-Mendez, S., 2021. Reusable Ag@TiO2-based photocatalytic nanocomposite membranes for solar degradation of contaminants of emerging concern. Polymers 13.
Bakshi, A., Panigrahi, A., 2018. A comprehensive review on chromium induced alterations in fresh water fishes. Toxicol Rep 5, 440–447.
Bilgiç, A., Çimen, A., 2019. Removal of chromium(vi) from polluted wastewater by chemical modification of silica gel with 4-acetyl-3-hydroxyaniline. RSC Adv. 9, 37403–37414.
Bora, A.J., Dutta, R.K., 2019. Removal of metals (Pb, Cd, Cu, Cr, Ni, and Co) from drinking water by oxidation-coagulation-absorption at optimized pH. J. Water Proc. Eng. 31, 100839.
Castellanos, N.J., Martinez Rojas, Z., Camargo, H.A., Biswas, S., Granados-Oliveros, G., 2019. Congo red decomposition by photocatalytic formation of hydroxyl radicals (·OH) using titanium metal–organic frameworks. Transit. Met. Chem. 44, 77–87.
Choi, H., Zakersalehi, A., Al-Abed, S.R., Han, C., Dionysiou, D.D., 2014. Chapter 8 - nanostructured titanium oxide film- and membrane-based photocatalysis for water treatment. In: Street, A., Sustich, R., Duncan, J., Savage, N. (Eds.), Nanotechnology Applications for Clean Water, second ed. William Andrew Publishing, Oxford, pp. 123–132.
Choong, C.E., Wong, K.T., Jang, S.B., Saravanan, P., Park, C., Kim, S.-H., Jeon, B.-H., Choi, J., Yoon, Y., Jang, M., 2021. Granular Mg-Fe layered double hydroxide prepared using dual polymers: insights into synergistic removal of As(III) and As(V). J. Hazard. Mater. 403, 123883.
Correia, D.M., Nunes-Pereira, J., Alikin, D., Kholkin, A.L., Carabineiro, S.A.C., Rebouta, L., Rodrigues, M.S., Vaz, F., Costa, C.M., Lanceros-Méndez, S., 2019. Surface wettability modification of poly(vinylidene fluoride) and copolymer films and membranes by plasma treatment. Polymer 169, 138–147.
Daradmare, S., Xia, M., Le, V.N., Kim, J., Park, B.J., 2021. Metal–organic frameworks/alginate composite beads as effective adsorbents for the removal of hexavalent chromium from aqueous solution. Chemosphere 270, 129487.
Dvoynenko, O., Lo, S.-L., Chen, Y.-J., Chen, G.W., Tsai, H.-M., Wang, Y.-L., Wang, J.-K., 2021. Speciation analysis of Cr(VI) and Cr(III) in water with surface-enhanced Raman spectroscopy. ACS Omega 6, 2052–2059.
Edet, U.A., Ifelebuegu, A.O., 2020. Kinetics, isotherms, and thermodynamic modeling of the adsorption of phosphates from model wastewater using recycled. Brick Waste. Processes 8, 665.
Efome, J.E., Rana, D., Matsuura, T., Lan, C.Q., 2018. Metal–organic frameworks supported on nanofibers to remove heavy metals. J. Mater. Chem. A 6, 4550–4555.
Fang, Y., Wen, J., Zeng, G., Jia, F., Zhang, S., Peng, Z., Zhang, H., 2018. Effect of mineralizing agents on the adsorption performance of metal–organic framework MIL-100(Fe) towards chromium(VI). Chem. Eng. J. 337, 532–540.
Far, H.S., Hasanzadeh, M., Nashtaei, M.S., Rabbani, M., Haji, A., Hadavi Moghadam, B., 2020. PPI-Dendrimer-Functionalized magnetic metal–organic framework (Fe3O4@MOF@PPI) with high adsorption capacity for sustainable wastewater treatment. ACS Appl. Mater. Interfaces 12, 25294–25303.
Fisher, M.R., 2018. Environmental Biology. Open Oregon Educational Resources.
Fiyadh, S.S., AlSaadi, M.A., Jaafar, W.Z.B., AlOmar, M.K., Fayaed, S.S., Mohd, N.S.B., Hin, L.S., El-Shafie, A., 2019. Review on heavy metal adsorption processes by carbon nanotubes. J. Clean. Prod. 230, 783–793.
Gao, K., Li, J., Chen, M., Jin, Y., Ma, Y., Ou, G., Wei, Z., 2021. ZIF-67 derived magnetic nanoporous carbon coated by poly(m-phenylenediamine) for hexavalent chromium removal. Separ. Purif. Technol. 277.
Ghani, U., Hussain, S., Noor ul, A., Imtiaz, M., Ali Khan, S., 2020. Laterite clay-based geopolymer as a potential adsorbent for the heavy metals removal from aqueous solutions. J. Saudi Chem. Soc. 24, 874–884.
Golmohamadpour, A., Bahramian, B., Shafiee, A., Ma'mani, L., 2018. Slow released delivery of alendronate using β-cyclodextrine modified Fe–MOF encapsulated porous hydroxyapatite. J. Inorg. Organomet. Polym. Mater. 28, 1991–2000.
Gopalratnam, V.C., Bennett, G.F., Peters, R.W., 1988. The simultaneous removal of oil and heavy metals from industrial wastewater by joint precipitation and air flotation. Environ. Prog. 7, 84–92.
Grandcolas, M., Lind, A., 2022. 3D-printed polyamide structures coated with TiO2 nanoparticles, towards a 360-degree rotating photocatalytic reactor. Mater. Lett. 307.

Guo, J., Wang, L., Tu, Y., Muhammad, H., Fan, X., Cao, G., Laipan, M., 2021. Polypyrrole modified bentonite nanocomposite and its application in high-efficiency removal of Cr(VI). J. Environ. Chem. Eng. 9, 106631.
Gupta, K., Joshi, P., Gusain, R., Khatri, O.P., 2021. Recent advances in adsorptive removal of heavy metal and metalloid ions by metal oxide-based nanomaterials. Coord. Chem. Rev. 445.
Hamoudi, S.A., Hamdi, B., Brendlé, J., 2018. Chapter 4.7 - removal of ions Pb2+ and Cd2 + from aqueous solution by containment geomaterials. In: Dincer, I., Colpan, C.O., Kizilkan, O. (Eds.), Exergetic, Energetic and Environmental Dimensions. Academic Press, pp. 1029–1043.
Hashemi, B., Rezania, S., 2019. Carbon-based sorbents and their nanocomposites for the enrichment of heavy metal ions: a review. Microchim. Acta 186, 578.
Hou, S., Wu, Y.-n., Feng, L., Chen, W., Wang, Y., Morlay, C., Li, F., 2018. Green synthesis and evaluation of an iron-based metal–organic framework MIL-88B for efficient decontamination of arsenate from water. Dalton Trans. 47, 2222–2231.
Hu, J., Lo, I., Chen, G., 2004. Removal of Cr (VI) by magnetite. Water Sci. Technol. 50, 139–146.
Ibrahim, A.H., El-Mehalmey, W.A., Haikal, R.R., Safy, M.E.A., Amin, M., Shatla, H.R., Karakalos, S.G., Alkordi, M.H., 2019. Tuning the chemical environment within the UiO-66-NH2 nanocages for charge-dependent contaminant uptake and selectivity. Inorg. Chem. 58, 15078–15087.
Kim, J., Benjamin, M.M., 2004. Modeling a novel ion exchange process for arsenic and nitrate removal. Water Res. 38, 2053–2062.
Langford, M., 2005. The United Nations concept of water as a human right: a new paradigm for old problems? Int. J. Water Resour. Dev. 21, 273–282.
Li, R., Li, N., Hou, J., Yu, Y., Liang, L., Yan, B., Chen, G., 2021. Aquatic environment remediation by atomic layer deposition-based multi-functional materials: a review. J. Hazard. Mater. 402, 123513.
Lopes, A.C., Gonçalves, R., Costa, C.M., Fonseca, A.M., Botelho, G., Neves, I.C., Lanceros-Mendez, S., 2012. Effect of zeolite content in the electrical, mechanical and thermal degradation response of poly(vinylidene fluoride)/NaY zeolite composites. J. Nanosci. Nanotechnol. 12, 6804–6810.
Mahmoud, M.E., El-Sharkawy, R.M., Ibrahim, G.A.A., 2021. Promoted adsorptive removal of chromium(vi) ions from water by a green-synthesized hybrid magnetic nanocomposite (NFe3O4Starch-Glu-NFe3O4ED). RSC Adv. 11, 14829–14843.
Mahmoud, M.E., Elsayed, S.M., Mahmoud, S.E.M.E., Aljedaani, R.O., Salam, M.A., 2022. Recent advances in adsorptive removal and catalytic reduction of hexavalent chromium by metal–organic frameworks composites. J. Mol. Liq. 347, 118274.
Mao, S., Shen, T., Han, T., Ding, F., Zhao, Q., Gao, M., 2021. Adsorption and co-adsorption of chlorophenols and Cr(VI) by functional organo-vermiculite: experiment and theoretical calculation. Separ. Purif. Technol. 277.
Martins, P.M., Ribeiro, J.M., Teixeira, S., Petrovykh, D.Y., Cuniberti, G., Pereira, L., Lanceros-Méndez, S., 2019a. Photocatalytic microporous membrane against the increasing problem of water emerging pollutants. Materials 12, 1649.
Martins, P.M., Ribeiro, J.M., Teixeira, S., Petrovykh, D.Y., Cuniberti, G., Pereira, L., Lanceros-Méndez, S., 2019b. Photocatalytic microporous membrane against the increasing problem of water emerging pollutants. Materials (Basel, Switzerland) 12.
Martins, P.M., Santos, B., Salazar, H., Carabineiro, S.A.C., Botelho, G., Tavares, C.J., Lanceros-Mendez, S., 2022. Multifunctional hybrid membranes for photocatalytic and adsorptive removal of water contaminants of emerging concern. Chemosphere 293, 133548.
Masudi, A., Harimisa, G.E., Ghafar, N.A., Jusoh, N.W.C., 2020. Magnetite-based catalysts for wastewater treatment. Environ. Sci. Pollut. Res. 27, 4664–4682.
Meena, A.H., Arai, Y., 2016. Effects of common groundwater ions on chromate removal by magnetite: importance of chromate adsorption. Geochem. Trans. 17, 1.
Murad, H.A., Ahmad, M., Bundschuh, J., Hashimoto, Y., Zhang, M., Sarkar, B., Ok, Y.S., 2022a. A remediation approach to chromium-contaminated water and soil using engineered biochar derived from peanut shell. Environ. Res. 204, 112125.
Murad, H.A., Ahmad, M., Bundschuh, J., Hashimoto, Y., Zhang, M., Sarkar, B., Ok, Y.S., 2022b. A remediation approach to chromium-contaminated water and soil using engineered biochar derived from peanut shell. Environ. Res. 204.
Nasrollahpour, A., Moradi, S.E., 2017. Hexavalent chromium removal from water by ionic liquid modified metal-organic frameworks adsorbent. Microporous Mesoporous Mater. 243, 47–55.
Ng, L.Y., Mohammad, A.W., Leo, C.P., Hilal, N., 2013. Polymeric membranes incorporated with metal/metal oxide nanoparticles: a comprehensive review. Desalination 308, 15–33.
Niu, H., Zheng, Y., Wang, S., He, S., Cai, Y., 2017. Stable hierarchical microspheres of 1D Fe–gallic acid MOFs for fast and efficient Cr(vi) elimination by a combination of reduction, metal substitution and coprecipitation. J. Mater. Chem. A 5, 16600–16604.
Pavithra, K.G., Jaikumar, V., Kumar, P.S., SundarRajan, P., 2019. A review on cleaner strategies for chromium industrial wastewater: present research and future perspective. J. Clean. Prod. 228, 580–593.
Priya, A.K., Yogeshwaran, V., Rajendran, S., Hoang, T.K.A., Soto-Moscoso, M., Ghfar, A. A., Bathula, C., 2022. Investigation of mechanism of heavy metals (Cr6+, Pb2+& Zn2+) adsorption from aqueous medium using rice husk ash: kinetic and thermodynamic approach. Chemosphere 286.
Rahmani, E., Rahmani, M., 2020. Catalytic process modeling and sensitivity analysis of alkylation of benzene with ethanol over MIL-101(Fe) and MIL-88(Fe). Front. Chem. Sci. Eng. 14, 1100–1111.
Rasheed, A., Carvalho, A.A.C., de Carvalho, G.G.A., Ghous, T., Nomura, C.S., Esposito, B. P., 2020. Chromium removal from aqueous solutions using new silica gel conjugates of desferrioxamine or diethylenetriaminepentaacetic acid. Environ. Sci. Pollut. Res. 27, 15635–15644.
Renu, Agarwal, M., Singh, K., 2016. Heavy metal removal from wastewater using various adsorbents: a review. J. Water Reuse Desalin. 7, 387–419.
Ribeiro, C., Costa, C.M., Correia, D.M., Nunes-Pereira, J., Oliveira, J., Martins, P., Gonçalves, R., Cardoso, V.F., Lanceros-Méndez, S., 2018. Electroactive poly (vinylidene fluoride)-based structures for advanced applications. Nat. Protoc. 13, 681–704.
Saiz, P.G., Iglesias, N., González Navarrete, B., Rosales, M., Quintero, Y.M., Reizabal, A., Orive, J., Fidalgo Marijuan, A., Larrea, E.S., Lopes, A.C., Lezama, L., García, A., Lanceros-Mendez, S., Arriortua, M.I., Fernández de Luis, R., 2020a. Chromium speciation in zirconium-based metal-organic frameworks for environmental remediation. Chemistry (Weinheim an der Bergstrasse, Germany) 26, 13861–13872.
Saiz, P.G., Iglesias, N., González Navarrete, B., Rosales, M., Quintero, Y.M., Reizabal, A., Orive, J., Fidalgo Marijuan, A., Larrea, E.S., Lopes, A.C., Lezama, L., García, A., Lanceros-Mendez, S., Arriortua, M.I., Fernández de Luis, R., 2020b. Chromium speciation in zirconium-based metal–organic frameworks for environmental remediation. Chem. Eur J. 26, 13861–13872.
Saiz, G., , P., Valverde, A., Gonzalez-Navarrete, B., Rosales, M., Quintero, Y.M., Fidalgo-Marijuan, A., Orive, J., Reizabal, A., Larrea, E.S., Arriortua, M.I., Lanceros-Méndez, S., García, A., Fernández de Luis, R., 2021. Modulation of the bifunctional CrVI to CrIII photoreduction and adsorption capacity in ZrIV and TiIV benchmark metal-organic frameworks. Catalysts 11, 51.
Salazar, H., Lima, A.C., Lopes, A.C., Botelho, G., Lanceros-Mendez, S., 2015. Poly (vinylidene fluoride-trifluoroethylene)/NAY zeolite hybrid membranes as a drug release platform applied to ibuprofen release. Colloids Surf. A Physicochem. Eng. Asp. 469, 93–99.
Salazar, H., Nunes-Pereira, J., Correia, D.M., Cardoso, V.F., Gonçalves, R., Martins, P.M., Ferdov, S., Martins, M.D., Botelho, G., Lanceros-Méndez, S., 2016. Poly(vinylidene fluoride-hexafluoropropylene)/bayerite composite membranes for efficient arsenic removal from water. Mater. Chem. Phys. 183, 430–438.
Salazar, H., Martins, P.M., Santos, B., Fernandes, M.M., Reizabal, A., Sebastián, V., Botelho, G., Tavares, C.J., Vilas-Vilela, J.L., Lanceros-Mendez, S., 2020. Photocatalytic and antimicrobial multifunctional nanocomposite membranes for emerging pollutants water treatment applications. Chemosphere 250, 126299.
Salazar, H., Martins, P.M., Valverde, A., Fernández de Luis, R., Vilas-Vilela, J.L., Ferdov, S., Botelho, G., Lanceros-Mendez, S., 2021. Reusable nanocomposite membranes for highly efficient arsenite and arsenate dual removal from water. Adv. Mater. Interfaces, 2101419 n/a.
Salazar, H., Martins, P.M., Valverde, A., Fernández de Luis, R., Vilas-Vilela, J.L., Ferdov, S., Botelho, G., Lanceros-Mendez, S., 2022. Reusable nanocomposite membranes for highly efficient arsenite and arsenate dual removal from water. Adv. Mater. Interfaces 9 (10), 101419 n/a.
Shen, W., Mu, Y., Xiao, T., Ai, Z., 2016. Magnetic Fe3O4–FeB nanocomposites with promoted Cr(VI) removal performance. Chem. Eng. J. 285, 57–68.
Singh, V., Singh, J., Mishra, V., 2021. Development of a cost-effective, recyclable and viable metal ion doped adsorbent for simultaneous adsorption and reduction of toxic Cr (VI) ions. J. Environ. Chem. Eng. 9.
Slater, C.S., Ahlert, R., Uchrin, C., 1983. Applications of reverse osmosis to complex industrial wastewater treatment. Desalination 48, 171–187.
Souza, A.D.V., Arruda, C.C., Fernandes, L., Antunes, M.L.P., Kiyohara, P.K., Salomão, R., 2015. Characterization of aluminum hydroxide (Al(OH)3) for use as a porogenic agent in castable ceramics. J. Eur. Ceram. Soc. 35, 803–812.
Speer, R.M., Wise, J.P., 2018. Current status on chromium research and its implications for health and risk assessment. In: Reference Module in Chemistry, Molecular Sciences and Chemical Engineering. Elsevier.
Sun, T., Liu, Y., Shen, L., Xu, Y., Li, R., Huang, L., Lin, H., 2020. Magnetic field assisted arrangement of photocatalytic TiO2 particles on membrane surface to enhance membrane antifouling performance for water treatment. J. Colloid Interface Sci. 570, 273–285.
Teixeira, S., Martins, P.M., Lanceros-Méndez, S., Kühn, K., Cuniberti, G., 2016. Reusability of photocatalytic TiO2 and ZnO nanoparticles immobilized in poly (vinylidene difluoride)-co-trifluoroethylene. Appl. Surf. Sci. 384, 497–504.
Valentín-Reyes, J., García-Reyes, R., García-González, A., Soto-Regalado, E., Cerino-Córdova, F., 2019. Adsorption mechanisms of hexavalent chromium from aqueous solutions on modified activated carbons. J. Environ. Manag. 236, 815–822.
Vinothkumar, K., Shivanna Jyothi, M., Lavanya, C., Sakar, M., Valiyaveettil, S., Balakrishna, R.G., 2022. Strongly co-ordinated MOF-PSF matrix for selective adsorption, separation and photodegradation of dyes. Chem. Eng. J. 428.
Wadhawan, S., Jain, A., Nayyar, J., Mehta, S.K., 2020. Role of nanomaterials as adsorbents in heavy metal ion removal from waste water: a review. J. Water Proc. Eng. 33, 101038.
WHO/UNICEF, 2019. Progress on Household Drinking Water, Sanitation and Hygiene 2000-2017: Special Focus on Inequalities.
Wu, S., Ge, Y., Wang, Y., Chen, X., Li, F., Xuan, H., Li, X., 2018a. Adsorption of Cr (VI) on nano Uio-66-NH2 MOFs in water. Environ. Technol. 39, 1937–1948.
Wu, S., Ge, Y., Wang, Y., Chen, X., Li, F., Xuan, H., Li, X., 2018b. Adsorption of Cr(VI) on nano Uio-66-NH2 MOFs in water. Environ. Technol. 39, 1937–1948.
Zango, Z.U., Jumbri, K., Sambudi, N.S., Hanif Abu Bakar, N.H., Fathihah Abdullah, N.A., Basheer, C., Saad, B., 2019. Removal of anthracene in water by MIL-88(Fe), NH2-MIL-88(Fe), and mixed-MIL-88(Fe) metal–organic frameworks. RSC Adv. 9, 41490–41501.
Zhang, S., Wang, J., Zhang, Y., Ma, J., Huang, L., Yu, S., Chen, L., Song, G., Qiu, M., Wang, X., 2021. Applications of water-stable metal-organic frameworks in the removal of water pollutants: a review. Environ. Pollut. 291.
Zhang, G., Yang, H., Li, Z., Jiang, M., Zhang, Q., 2022. Comparative investigation on removal of thallium(I) from wastewater using low-grade pyrolusite and pyrolysis

residue derived from oily sludge: performance, mechanism and application. Groundwater Sustain. Dev. 16, 100713.
Zhou, T., Liang, Q., Zhou, X., Luo, H.J., Chen, W., 2021. Enhanced removal of toxic hexavalent chromium from aqueous solution by magnetic Zr-MOF@polypyrrole: performance and mechanism. Environ. Sci. Pollut. Res. 28, 13084–13096.
Zhou, H., Ye, M., Zhao, Y., Baig, S.A., Huang, N., Ma, M., 2022. Sodium citrate and biochar synergistic improvement of nanoscale zero-valent iron composite for the removal of chromium (VI) in aqueous solutions. J. Environ. Sci. (China) 115, 227–239.
Zhu, F., Zheng, Y.-M., Zhang, B.-G., Dai, Y.-R., 2021. A critical review on the electrospun nanofibrous membranes for the adsorption of heavy metals in water treatment. J. Hazard. Mater. 401, 123608.
Zinicovscaia, I., Safonov, A., Boldyrev, K., Gundorina, S., Yushin, N., Petuhov, O., Popova, N., 2020. Selective metal removal from chromium-containing synthetic effluents using Shewanella xiamenensis biofilm supported on zeolite. Environ. Sci. Pollut. Res. 27, 10495–10505.
Zioui, D., Salazar, H., Aoudjit, L., Martins, P.M., Lanceros-Méndez, S., 2020. Polymer-based membranes for oily wastewater remediation. Polymers 12, 42.